JOURNAL OF APPLIED CRYSTALLOGRAPHY
ISSN 1600-5767

# *FullProfAPP*: a graphical user interface for the streamlined automation of powder diffraction data analysis

Oier Arcelus,[a,b]* Juan Rodríguez-Carvajal,[c]* Nebil A. Katcho,[c] Marine Reynaud,[a] Ashley P. Black,[b] Dimitrios Chatzogiannakis,[b,a,d] Carlos Frontera,[b] Jon Serrano-Sevillano,[a] Maha Ismail,[a,e] Javier Carrasco,[a,f] Francois Fauth,[g] M. Rosa Palacin[b] and Montse Casas-Cabanas[a,f]

[a]Centre for Cooperative Research on Alternative Energies (CIC energiGUNE), Basque Research and Technology Alliance (BRTA), Alava Technology Park, Albert Einstein 48, 01510 Vitoria-Gasteiz, Spain, [b]Institut de Ciència de Materials de Barcelona, ICMAB-CSIC, Campus de la UAB, 08193 Bellaterra, Spain, [c]Diffraction Group, Institut Laue–Langevin, 71 Avenue des Martyrs, CEDEX 9, F-38054 Grenoble, France, [d]Alistore ERI, CNRS FR 3104, France, [e]Physical Chemistry Department, Pharmacy Faculty, University of the Basque Country, 01006 Vitoria-Gasteiz, Spain, [f]IKERBASQUE, Basque Foundation for Science, Plaza Euskadi 5, 48009 Bilbao, Spain, and [g]CELLS-ALBA Synchrotron, Cerdanyola del Vallès, 08290 Barcelona, Spain. *Correspondence e-mail: oarcelus@cicenergigune.com, rodriguez-carvajal@ill.fr

Received 10 April 2024
Accepted 13 July 2024

Edited by A. H. Liu, HPSTAR and Harbin Institute of Technology, People's Republic of China

**Keywords:** Rietveld refinement; software; graphical user interfaces; *FullProf*; high-throughput data handling; sequential refinements; powder diffraction.

**Supporting information:** this article has supporting information at journals.iucr.org/j

*FullProfAPP* is a software tool for data processing, refinement and visualization of large collections of powder diffraction patterns. Featuring an intuitive graphical user interface, it seamlessly facilitates a variety of tasks. These include conducting full-profile phase searches, sequential and high-throughput Rietveld refinements, and managing background (and peak) detection. *FullProfAPP* also provides convenient interaction with crystallographic databases and supports the visualization and export of high-quality pixel and vector graphics depicting the refinement results, among other functionalities. *FullProfAPP* wraps around the refinement program *FullProf* [Rodríguez-Carvajal (1993), *Physica B*, **192**, 55–69] and offers the flexibility of user-defined workflows by accessing and editing *FullProf*'s input files and triggering its execution as necessary. *FullProfAPP* is distributed as open-source software and is presently available for Windows and Linux operating systems.

## 1. Introduction

Powder diffraction is a fundamental technique in materials science for the study of crystalline solids. It is essential in guiding experimental research by providing insights into the crystal structure, composition, purity, degree of disorder and microstructural information of materials, among other properties. Typically, experimental diffraction patterns are initially qualitatively analysed to identify peak positions, intensities and peak profiles. Subsequently, the phases present in the experimental samples are identified, peaks are indexed, and the refinement of the pattern's profile is conducted using methods such as those developed by Le Bail *et al.* (1988) or Rietveld (1969). This entails starting from an initial calculation of a powder diffraction pattern and iteratively optimizing the model's parameters by comparing the calculated patterns with experimental data. This optimization procedure enables the extraction of precise quantitative information about the structural, compositional and microstructural characteristics of the samples. The refinement process is assisted by refinement engines like *FullProf* (Rodríguez-Carvajal, 1993), which require significant user intervention and expert guidance. The quality of the refinement also relies on the data and

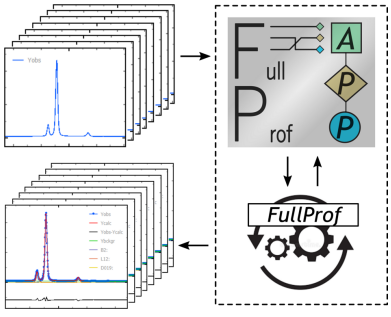

refinement strategy employed, making it challenging to determine, *a priori*, the best parameter refinement order.

This relatively manual process contrasts with the increasing rate of powder diffraction data collection in recent years. This surge is primarily driven by the rise of materials discovery research through high-throughput screening (Curtarolo *et al.*, 2013) and *in situ* and *operando* experiments (Liu *et al.*, 2019; Saurel *et al.*, 2021) which follow the evolution of the sample under study in dynamic conditions. The adoption of materials acceleration platforms (Flores-Leonar *et al.*, 2020; Castelli *et al.*, 2021; Stier *et al.*, 2023; Lombardo *et al.*, 2022) and the increased access to large-scale user facilities such as synchrotrons and neutron sources (Wang *et al.*, 2018; Atkins *et al.*, 2022; Saurel *et al.*, 2021) are expected to fuel this trend. Consequently, there is a pressing need for software tools that can efficiently accelerate the analysis and processing of data, thereby facilitating an increased rate of scientific discovery. Another crucial consideration is the democratization of access to highly automated and large-scale experiments. This entails that the user base should have seamless on-site interaction with the software infrastructure. This accommodation is essential for users with diverse skill levels, including individuals who may not possess specialized skills in software development or scripting. By eliminating this potential obstacle, the efficient utilization of such platforms can be ensured.

One way to address this issue is to build graphical user interfaces (GUIs) that facilitate the use of the underlying logic and programs. In the context of powder diffraction pattern refinements, notable examples include commercial packages such as *JADE* (Jennings, 2021) and *TOPAS* (Coelho, 2018), or academic packages such as *GSAS-II* (Toby & Von Dreele, 2013), *Profex* (Doebelin & Kleeberg, 2015), *MAUD* (Lutterotti, 2010) and *FullProf* (Rodríguez-Carvajal, 1993). This last is included in the *FullProf Suite*, a set of crystallographic programs that provide GUIs, such as *WinPLOTR* (Roisnel & Rodríquez-Carvajal, 2001), for visualization, Rietveld analysis, and pre- and post-processing of neutron and X-ray diffraction data. Other programs, such as *Sr.Rietveld* (Tian *et al.*, 2013) and *AutoFP* (Cui *et al.*, 2015), offer GUIs with extended functionalities, which are specifically designed to facilitate refinement strategies for batches of experimental patterns. However, to the best of our knowledge, these programs are not compatible with modern versions of Python and have not been actively maintained for several years.

Considering all the above-mentioned points, the *FullProfAPP* software is presented here. This application, built in Python, acts as a wrapper for the *FullProf* software. It provides a user-friendly GUI and offers a high-level abstraction layer that enables the utilization of highly automated and flexible refinement workflows. With *FullProfAPP*, users can easily access and make use of all the capabilities of *FullProf* through a streamlined and intuitive interface. The software aims to simplify the refinement process by automating various tasks such as full-profile phase searches, sequential refinements using data derived from *operando* and/or *in situ* experiments, and refinement of large amounts of data resulting from high-throughput experiments, while providing a more user-friendly experience. Yet, *FullProfAPP* still allows users to access and manipulate the actual data and input files, enabling further processing with other utilities available in the *FullProf Suite*. *FullProfAPP* implements various functionalities by exploiting modern and efficient libraries to perform the data treatment and visualization of both experimental and calculated patterns. It incorporates full-profile phase search algorithms and highly automated refinements of batches of diffraction patterns with customizable workflows. These algorithms are distributed across multiple concurrent processes, harnessing the computational power of modern multicore computers and workstations to parallelize batch refinements and full-profile phase search tasks. Furthermore, it includes a client that interacts with materials databases, providing users with the ability to download crystallographic information files (CIFs) directly through the GUI. As of the present date, *FullProfAPP* is available in Windows and Linux operating systems.

## 2. The *FullProfAPP* program

### 2.1. Structure of the program

*FullProfAPP* is built around the refinement engine *FullProf* (Rodríguez-Carvajal, 1993). It efficiently manages input/output (I/O) data streams and executes the necessary commands to seamlessly operate a variety of Rietveld refinement workflows on powder diffraction data sets. The structure of the program is shown in Fig. 1, providing a clear overview of its components and their interconnections. In the following, a detailed description of the program's structure is given, outlining its key elements and their functionalities (as implemented in Version 1.2.3). The GUI is the component that controls the functionality of the program. It is implemented using *PyQt5* (https://riverbankcomputing.com/software/pyqt/intro), a Python wrapper for *Qt*, which is a popular C++ library

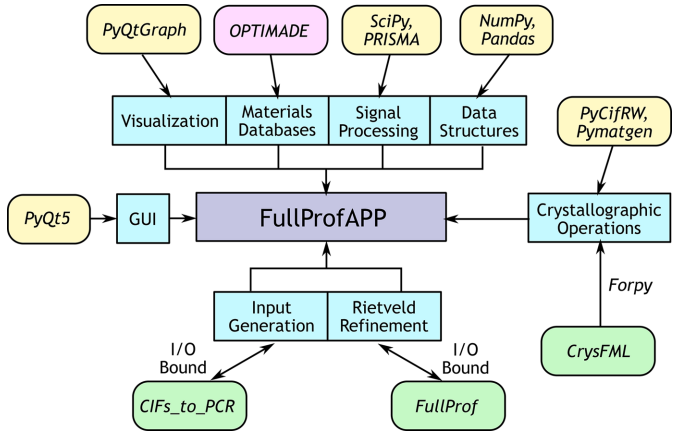


**Figure 1**
The components of the *FullProfAPP* software. Right-angled rectangles indicate functionality, while rounded rectangles indicate the libraries, programs or APIs that the functionality depends on. A yellow background indicates that the software piece is written in (or aimed to be used in) Python. A green background indicates code written in Fortran. A pink background indicates a generic response format (JSON in this case).

for GUI development. With the GUI, users can perform the following tasks:

(i) Visualize the powder diffraction data and refinement results. The visualization functionality is provided by *PyQtGraph* (https://www.pyqtgraph.org/), a scientific graphics library built for Python. *PyQtGraph* excels in terms of speed and performance, making it an ideal choice for rendering and displaying scientific data, especially when presented in large sets. It offers smooth real-time interactivity with 2D graphs and straightforward support for *PyQt5*-based applications. Therefore, *PyQtGraph* is the natural choice for a graphics library for *FullProfAPP*.

(ii) Process the diffraction data to extract the background signal and peak positions and intensities. The background signal is fitted using the asymmetric least-squares smoothing method (Eilers, 2003) as implemented in the *PRISMA* software (Flores *et al.*, 2022). Peak positions and intensities are extracted using one of *SciPy*'s (https://scipy.org/) peak-finder algorithms. The GUI enables easy variation of the method's input parameters, allowing the user to have immediate feedback on the resulting background shapes and peak positions.

(iii) Interact with the Crystallography Open Database (COD; http://www.crystallography.net/cod/) through *OPTIMADE* (Andersen *et al.*, 2021), an application programming interface (API) with a common specification for several materials databases. *FullProfAPP* allows users to download CIFs containing the necessary information to perform subsequent Rietveld refinements using the *CIFs_to_PCR* program as implemented in the *FullProf Suite*.

(iv) Refine the loaded experimental patterns using the Rietveld method as implemented in *FullProf*. *FullProfAPP* offers several workflows that achieve a variety of tasks, such as full-profile phase searches on the downloaded CIFs; simulation of X-ray diffraction or neutron powder diffraction profiles for preliminary visual checks on the experimental data; manual and automated Rietveld refinements where users can select flexible workflows for the refinement order; and sequential refinements where those flexible workflows are run along the pattern series, largely preventing refinement divergences. While most operations related to the pattern's refinements are I/O bound, some internal crystallographic calculations are also done using the *CrysFML* library (Rodriguez-Carvajal & Gonzalez-Platas, 2002) and interfaced with *FullProfAPP* through *Forpy* (https://ylikx.github.io/forpy/index.html). The following sections offer more details and examples for the above-mentioned workflows.

The application is distributed under the GNU General Public Licence Version 3 (GPLv3). The program can be downloaded from either the BIG-MAP AppStore (https://big-map.github.io/big-map-registry/), the *FullProf* website (https://www.ill.eu/sites/fullprof/) or CIC energiGUNE's webpage (https://cicenergigune.com/en/fullprof-app). Within the distribution, installers for both Linux and Windows are provided, such that the user has no need to install a Python interpreter with all the dependencies and can readily use *FullProfAPP*. However, users will still need to keep the *FullProf Suite* updated to the latest version. The source code is found in the GitLab repository at https://gitlab.com/d7081/fullprofapp. Documentation showing the details of the GUI and working examples can be found on the website https://fullprofapp.readthedocs.io/en/stable.

### 2.2. The GUI

The application's main window is divided into four sections (Fig. S1 in the supporting information), the toolbar, the graphics area, the terminal and materials area, and the protocols and file system area. Each of these sections is resizable by dragging splitters that exist within the areas.

**2.2.1. Toolbar.** The toolbar contains four menus, 'File', 'Pattern', 'Materials' and 'View'. The 'File' menu is used to select the working directory for the project, save the current state or load a previous state of the application. All the data generated by *FullProfAPP* are saved in the working directory and classified into folders that are named after the type of job, *i.e.* `FPSEARCH`, `MANUAL`, `FPAUTO` and `FPSEQ` for phase searches and manual, automatic and sequential refinements, respectively. Each job type is described in detail in the following sections. The loading/saving of the application state is done through an INI file with a `.fpapp` extension. This file can be loaded through the 'File' menu or directly with a double click on the file in the Windows or Linux file manager.

The 'Pattern' menu is used to load, edit and export experimental powder diffraction patterns, backgrounds and peak information. The 'Import Patterns' action allows the user to load one or many diffraction patterns in different formats. The use of an instrumental resolution function (IRF, available in different formats, see Section S1 in the supporting information for a full description) to account for instrumental profile parameters is mandatory to work with the current version of *FullProfAPP*. The 'Automatic Background' and 'Peak Detection' actions are used to extract background points from the experimental patterns and detect peak positions and intensities, which can be edited by activating the 'Edit Background' or 'Edit Peaks' modes. Lastly, the 'Export Background' and 'Export Peaks' actions allow the user to export background and peak information to a text file for later use.

The 'Materials' menu enables two actions. The 'Search in Remote Database' action allows the user to filter crystallographic phases in the COD, download their corresponding CIFs into the working directory and load them into the application. For example, by searching for phases that are known to contain {Fe, O} while optionally considering the inclusion of {Li, P}, the application can automatically download all CIFs in the Fe–O phase diagram and retrieve those phases that also involve Li or P. However, recognizing that sometimes the querying criteria provided by the application may be too general, resulting in long waiting times, or that users may possess their own CIFs, *FullProfAPP* also offers the flexibility to search for a collection of CIFs within the user's drives. In that case, the 'Search in Local Database' action allows users to select CIFs that are already stored on their system.

Lastly, the 'View' menu contains actions that allow visualization of the results of the Rietveld refinement jobs. The actions 'Current (.prf)' and 'Current (WinPLOTR)' plot the profiles resulting from the most recent refinement process inside the graphics area or from executing *WinPLOTR* (Roisnel & Rodríquez-Carvajal, 2001), respectively. The actions 'Select (.prf)' and 'Select (WinPLOTR)', on the other hand, plot the refined profiles from any other folder in the system. The 'Current Results (.mic/.sum)' and 'Select Results (.mic/.sum)' actions plot a summary of the results obtained from the refinements, such as weight fractions, cell parameters and atomic positions, amongst others.

**2.2.2. Graphics area.** The graphics area contains all the functionalities for the visualization of the experimental data and the results from the refinement runs. It contains tabbed sections that are shown at different stages of the analysis. The first 'Exp. Data' tab is always visible and contains the loaded experimental patterns, as well as the background points and peak positions and intensities (if requested). The 'Prf Data' and 'Summary' tabs are hidden at the start but become visible after the first successful run of a Rietveld refinement. In particular, the 'Prf Data' tab shows the experimental profiles superimposed on the total calculated profiles, the individual phase profiles, the difference between experimental and calculated profiles, and the positions of the *hkl* reflections. The 'Summary' tab, on the other hand, gathers and visualizes important parameters that result from the refinement runs. A tickable parameter tree is implemented that allows the user to select parameters of interest for further visualization and analysis.

This area also contains a small toolbar which is meant to help the user navigate between all the patterns and refined profiles that are loaded into the application. This toolbar contains the 'Pattern Checks' menu, which acts as a selector for loaded patterns that can be chosen for further analysis. In short, the patterns that are marked as 'ticked' will be used in subsequent refinement jobs, while those marked as 'unticked' will be disregarded. However, there is one exception to this rule when it comes to sequential refinements. In sequential refinements, *FullProfAPP* searches for the first pattern file that is marked as 'ticked' and utilizes its refinement data as the input for the next pattern's refinement. This process continues until there are no more patterns to refine or until the last 'ticked' pattern is found. The following sections will delve into further details about this process, providing a more comprehensive understanding of its operation and implications.

Additionally, the 'Contour Plot' button located in the toolbar allows the user to plot contours easily on the loaded data. It allows playing with the colour scale by moving the mouse wheel and adding 'Ctrl' and 'Shift' modifiers to select upper and lower bounds of the colour scale, respectively.

**2.2.3. Terminal and materials area.** The terminal and materials area contains the following tabs: 'Terminal', 'Queried Materials', 'Selected Materials' and 'Results'. The 'Terminal' tab contains a display that allows the user to obtain information about the state of execution of the programs that are run in the background, such as *FullProf* and *CIFs_to_PCR*. It also contains the 'Kill' and 'Clear' buttons, which immediately stop the processes that run in the background and clear the display text, respectively.

The 'Queried Materials' tab includes a table that contains crystallographic information from the CIFs that were loaded with the 'Search in Remote Database' or 'Search in Local Database' actions (see Section 2.2.1). The user can inspect the contents of each CIF that correspond to each row on the table by double clicking on the table items. The user can also filter the table entries by coincidence of the text that is written in the editable text section above. Additionally, this tab includes 'Submit Selection' and 'Simulate Selection' buttons. The former saves the selected phases from the 'Queried Materials' tab into the 'Selected Materials' tab, which are then going to be used in subsequent refinements. The latter, on the other hand, prepares *FullProf* simulations of the selected phases and compares them with the experimental pattern that is currently plotted as a reference.

Lastly, the 'Results' tab includes an additional table containing some basic information on the selected phases after a successful Rietveld refinement run.

**2.2.4. File system and Protocols area.** This area contains two tabs, 'File System' and 'Protocols'.

The 'File System' tab shows the folder and file structure of the working directory, where it is possible to inspect the contents of the files or delete them by interacting with the 'Show File' and 'Delete' actions that appear by right-clicking on the items.

The 'Protocols' tab contains expandable buttons that contain parameter fields and utilities that are necessary to run the corresponding Rietveld refinement protocols. These protocols achieve a variety of tasks by making *FullProfAPP* automatically run Rietveld refinement jobs in a controlled way using *FullProf*. *FullProfAPP* implements three options, 'Full-Profile Phase Search Protocol', 'Automatic Refinement Protocol' and 'Manual Refinement'. The next section provides detailed information for each of these protocols.

### 2.3. Protocols

**2.3.1. Full-Profile Phase Search Protocol.** As the name of the section indicates, *FullProfAPP* implements the full-profile search–match algorithm originally devised by Lutterotti *et al.* (2019). Unlike traditional search–match approaches, this protocol uses the Rietveld method to discern the constituent phases of the experimental samples. While a detailed description of the method can be found in the original paper, the main aspects of the algorithm and the small variations in the program's implementation are introduced in the following.

In this protocol, the set of candidate phases $S_1 = \{p_1, \ldots, p_N\}$ and an initially empty set of detected phases $S_2 = \{\ \}$ are defined. Regarding the Rietveld refinement process, two distinct types are used. The first type focuses on fast refinements and is used in the scanning step. The second type, which employs more stringent fitting criteria, is used to quantify phase fractions. The order in which the model parameters are refined remains the same for both types of refinement and

proceeds as follows. Initially, the scale factors are refined. Subsequently, if the weight fractions of the phases fall below a user-specified threshold ($f_{R0}$), those phases are not considered further in the refinement process. Next, if the weight fractions of the remaining phases surpass another weight fraction threshold ($f_{R1}$), the program proceeds to refine the cell parameters and constant $2\theta$ shifts. Finally, the crystallite size and strain parameters are refined, as well as the overall isotropic displacement parameters, for weight fractions larger than a third threshold ($f_{R2}$).

This algorithm runs fast refinements for each phase in $S_1$. Each phase is then ranked according to the following custom figure of merit (FoM):

$$\mathrm{FoM}^p = \left[\frac{1}{R_{\mathrm{wp}} + a v_0^p \left|(1/v_{\mathrm{r}}^p) - (1/v_0^p)\right|} + b(100 - f_{\mathrm{r}}^p)\right] \times \left(1 + \frac{c}{\langle D^p \rangle} + d\langle \varepsilon^p \rangle\right)^{-1}.$$

Here, the FoM has been adapted to work with *FullProf*. $R_{\mathrm{wp}}$ is the weighted profile factor, $v_{\mathrm{r}}$ ($v_0$) is the refined (initial) cell volume, $f_{\mathrm{r}}$ is the weight fraction, $\langle D \rangle$ is the average apparent crystallite size and $\langle \varepsilon \rangle$ is the average maximum strain. The superscript $p$ indicates that the values correspond to a phase in $S_1$ that is being evaluated in the refinement cycle. The parameters $a$, $b$, $c$ and $d$ are weighting coefficients that alter the value of the FoM in favour of phases that fulfil certain conditions. The parameters $c$ and $d$ become zero if $\langle D \rangle > D_{\mathrm{min}}$ and $\langle \varepsilon \rangle < \varepsilon_{\mathrm{max}}$, respectively, where $D_{\mathrm{min}} = 20$ Å and $\varepsilon_{\mathrm{max}} = 0.02(\pi/2)^{1/2}$ (see the description of the microstructure in Section S1 of the supporting information).

After all phases of $S_1$ have been scanned, the phase with the highest FoM is removed from $S_1$ and appended to $S_2$. Additionally, if the weight fractions that resulted from the scan are smaller than a certain threshold ($f_{S1}$), those phases are also suppressed from $S_1$. At this point, only a single phase is present in $S_2$. The algorithm continues by scanning all the remaining phases in $S_1$ with the one that was newly added to $S_2$ and, once more, taking the highest-FoM phase from $S_1$ and including it in $S_2$. Before including the new phase, the program checks for duplicated phases that may already exist in $S_2$. Here, two phases are considered as duplicated if the similarity index (de Gelder *et al.*, 2001) between their respective calculated diffraction profiles is above a predefined threshold. If this is the case, the phase is not included in $S_2$ but it is still removed from $S_1$. Then, the phase with the next highest FoM is considered and the same checks are performed. After a new phase is accepted, *FullProfAPP* initiates a quantification Rietveld refinement of the phases in $S_2$, aimed at achieving a more precise fit and obtaining accurate values for the phase weight fractions. If the quantification results in phases with weight fractions that fall below the threshold ($f_{S0}$), those phases are eliminated from $S_2$. At this point, *FullProfAPP* proceeds to start another cycle to select the next phase from $S_1$ to be added to the refinement process.

This whole process is repeated until one of the following conditions is met: (i) the last phase that was added to $S_2$ is removed because its weight fraction is below the threshold $f_{S0}$, (ii) there are no more phases in $S_1$ or (iii) the number of phases in $S_2$ is over a certain limit. Since the Rietveld refinements are performed one phase at a time, *FullProfAPP* is designed to capture refinement errors effectively from the *FullProf* standard output stream. In this case, if the errors originate from the scanning Rietveld step of $S_1$, the FoMs of the related phases are set strictly to zero, meaning that they will rank last in subsequent steps. Similarly, if the error originates during the quantification step, the cause of the error is assigned to the last phase that entered $S_2$. In such cases, the problematic phase is eliminated from the list and the search–match algorithm is terminated.

**2.3.2. Automatic Refinement Protocol.** This is the most general way of using *FullProfAPP*. This protocol window provides several functionalities for the user to perform Rietveld refinements in flexible user-defined refinement sequences. The protocol window is mainly divided into two sections, 'Patterns' and 'Workflow'.

The 'Patterns' section is used to load the refinement parameters (instrumental parameters, background, profile parameters, crystal structure *etc.*), linking them to the experimental patterns that were selected using the 'Pattern Checks' selector menu (see Section 2.2.2). These refinement parameters can be loaded from an existing PCR file (standard *FullProf* input file) or can be generated using the phases present in the 'Selected Materials' tab (see Section 2.2.3) and the background from the graphics area. This is achieved by executing the program *CIFs_to_PCR*.

Once all the necessary input information is loaded and linked to the corresponding experimental diffraction patterns, the Rietveld refinement strategy can be selected in the 'Workflow' section (Fig. S2). The selection of the refinement sequence is done using the tickable parameter tree. The items on the tree correspond to refinable parameters, and expanding the tree items will show the phases and crystallographic sites to which the refinements will be applied. Checking the items in the tree and selecting them as part of the workflow will update the panel to the right of the tree and show all the parameters that are set to be refined and the ones that are set fixed. The user can add further steps to the refinement by subsequently ticking items in the tree and selecting them as part of the workflow. *FullProfAPP* will then run this user-defined refinement process for each of the experimental patterns that were selected for processing.

*FullProfAPP* gives several options to tune the Rietveld analysis further. For instance, users can impose soft linear constraints between two or more parameters. In this case, the refinement procedure tries to fulfil the condition that the linear relation between the selected parameters, scaled by some user-defined coefficients, is equal to a given value within a tolerance. Users can also define hard constraints between the refinement parameters. In this case, the constrained parameters are forced to change according to the coefficients given by the user. For example, if two parameters are related by

coefficients 1.0 and −1.0, any increase in the value of the former must be matched with an equal decrease in the value of the latter.

Users can select the 'Profile Matching' mode in a particular phase if no information about the crystal structure is available. *FullProfAPP* offers two ways of performing the 'Profile Matching' analysis. The first one uses constant scale factors, meaning that the LeBail fitting method (Le Bail *et al.*, 1988) is applied. The second option uses constant relative intensities that are initially fed from a structure factor file (`.hkl`) and allows for the scale factor of the phase to be refined.

The 'Automatic Refinement Protocol' window can also be used to treat sequential data. Here, when the 'Sequential Mode' box is ticked, *FullProfAPP* assumes that the loaded experimental patterns constitute a series in which the refinement parameters of a particular pattern are related to those of the previous pattern within the sequence (*e.g.* temperature ramps, electrochemistry or similar scenarios). The user can interact with the protocol window exactly as explained above, but keeping in mind that there are some differences in the handling of the loaded patterns. For example, in contrast to the default mode, where only those patterns that were selected in the 'Pattern Checks' selector menu (see Section 2.2.2) would be treated, if the sequential mode is activated all the patterns between the first and last selected ones will be considered. In this case, the selected patterns work as 'checkpoints' that the user can employ to mark parts of the pattern series where qualitative differences appear with respect to the starting point, such as the appearance of a new phase. The user can first focus on these 'checkpoints' to provide well refined initial parameters, and then *FullProfAPP* will check for all unique phases that may appear between 'checkpoints' and prepare a single input file to be run in sequence. *FullProfAPP* connects the input parameters of the current pattern's refinement with the output parameters of the previous pattern, and it additionally monitors the weight fractions of the studied phases to automatically switch off the refinement of those that fall below a 2% threshold, which allows for sequential refinements that are robust and effective in avoiding divergences.

**2.3.3. Manual Refinement.** The 'Manual Refinement' window allows users to interact with the input refinement parameters in the same way they would with a text editor for typical *FullProf* PCR files. In fact, *FullProfAPP* shows most of the contents of the loaded PCR files formatted in tables that contain editable cells. In order to minimize the common errors that occur when editing the values and flags of the PCR files, some cells are kept fixed while others react automatically to the user's changes (*e.g.* number of background points, number of excluded regions or number of crystallographic sites). Some of the tables contain tickable boxes that activate additional refinement parameters and modes. Among these, *FullProfAPP* supports the following options: (i) micro-absorption parameters; (ii) parameters necessary for bond-valence sum calculations; (iii) phase-dependent constant $2\theta$ shifts, which are useful when the phases that contribute to the diffraction pattern are at different optical centres of the diffractometer, such as with samples formed of several polycrystalline thin films; (iv) anisotropic displacement parameters for the crystallographic sites; (v) anisotropic strain broadening and Lorentzian strain broadening; and (vi) anisotropic size broadening with the spherical harmonic expansion. The last two depend on the specific Laue class of the phase, which is inferred from the space group, and the corresponding parameters are automatically updated in the 'Manual Refinement' window.

Before delving further into the use cases and examples for *FullProfAPP*, it is important to acknowledge that *FullProfAPP* has certain limitations and may not be suitable for handling more advanced analyses that require specialized knowledge of *FullProf*, such as symmetry modes, magnetic structure refinements, single-crystal diffraction and others. In such cases the user must default to interacting directly with *FullProf* through the *FullProf Suite*. Thus, *FullProfAPP* should be viewed as a user-friendly interface that automates and extends functionality for high-throughput powder data treatment, and helps ease the entrance barrier for those users who need a fast and easy way of handling their data with *FullProf*.

## 3. Examples

In the following, we present the different functionalities of *FullProfAPP*. As already stated, *FullProfAPP* always requires the user to work with an IRF file. We recommend reading the corresponding text in the supporting information (Section S1) to obtain more information about the defaults that *FullProfAPP* uses to run Rietveld refinements with *FullProf*.

### 3.1. Egyptian makeup pigments

This example demonstrates a full-profile phase search conducted on an Egyptian makeup pigment sample using the methodologies presented in Section 2.3.1. The pigments discussed in the original work (Walter *et al.*, 1999) dated from the period between 2000 and 1200 BC. Rietveld analysis of the X-ray powder diffraction patterns revealed the presence of naturally occurring minerals like galena (PbS), cerussite ($PbCO_3$) and gypsum ($CaSO_4{\cdot}2H_2O$), alongside synthetic compounds such as laurionite (PbOHCl) and phosgenite ($Pb_2Cl_2CO_3$). The diffraction patterns were obtained on the DW22 beamline of the LURE laboratory (Orsay, France; $\lambda$ = 0.9627 Å). To build the list of candidate phases, a series of CIFs were downloaded using the 'Search in Remote Database' action in the 'Materials' menu (see Section 2.2.1). The CIFs were downloaded from the COD, restricting the composition to phases that contained either Pb or Ca, and that optionally contained C, O, S or Cl. After eliminating bad entries, such as phases with low symmetry (*e.g.* $P1$ or $P\overline{1}$) and unspecified space groups, a total of 366 phases were selected as candidates for the phase search process.

The *FullProfAPP* implementation of the search–match algorithm of Lutterotti *et al.* (2019) correctly detects the phases that were originally reported (Walter *et al.*, 1999).

**Table 1**
Egyptian makeup samples: results of the search–match algorithm on the 366 candidate phases downloaded from the COD, including phases with a composition containing Pb or Ca, and optionally containing C, O, S or Cl.

| Phase | COD ID | Formula | Space group | Weight fraction (%) | Weight fraction (%) (manual) |
|---|---|---|---|---|---|
| Laurionite | 9008250 | PbOHCl | *Pcmn* | 38.68 | 38.89 |
| Cerussite | 5000208 | $PbCO_3$ | *Pmcn* | 21.95 | 21.32 |
| Phosgenite | 9009573 | $Pb_2Cl_2CO_3$ | *P4/mbm* | 16.97 | 17.41 |
| Galena | 9008694 | PbS | $Fm\bar{3}m$ | 4.6 | 4.73 |
| Gypsum | 2300258 | $CaSO_4{\cdot}2H_2O$ | *I*12/*c*1 | 17.80 | 17.65 |

Table 1 and Fig. 2 show the results of the phase search analysis. Overall, the analysis conducted on a Hewlett–Packard 250G8 Notebook personal computer (Intel Core i5-1135 G7 at 2.4 GHz with 16 GB RAM) took approximately 6 min to complete, ensuring accurate operation of the search–match algorithm with a complex phase mixture within a reasonable time frame. This is, however, considerably longer than the timings reported in the original work for candidate lists of similar size. The reasons for this slower time are multifold: (i) the workstation used for the analysis is considerably less powerful than the setup used in the original work, resulting in slower processing times; (ii) there is a significant overhead associated with the execution of *FullProf* and the updating of the GUI state, which can make the overall process I/O bound, again leading to slower execution times; and (iii) each *FullProf* execution requires preparing the corresponding input PCR files, thus further slowing the analysis. We also note that the results of the refinements can be improved by taking a more careful and manual approach (Fig. S3). Nevertheless, the resulting weight fractions are very close to those obtained with the search–match algorithm.

We argue that this 'brute force' approach will hardly ever be the best solution to a sensible phase search analysis on powder patterns containing unknown phases. Instead, first pre-screening the candidate phases with the traditional search–match approach [as implemented in programs such as *Match!* (https://www.crystalimpact.com/match/) or Bruker's *Diffrac. EVA*] and then performing a full profile phase search is probably more efficient, especially when dealing with well crystallized laboratory-synthesized samples, where the set of possible phases is much more limited. However, we believe that *FullProfAPP* can become a powerful assistant when the user aims to screen automatically a series of dozens of patterns belonging to a given chemical system (*e.g.* high-throughput exploration of compositions or synthesis conditions within a defined chemical space), where the expected phases and possible secondary phases and impurities can be predicted by the user.

### 3.2. *Operando* studies

**3.2.1. Two-phase reaction between $LiFePO_4$ and $FePO_4$ under battery operation.** This section describes experiments carried out on the hard X-ray absorption and powder diffraction beamline BL16-NOTOS of the ALBA Synchrotron with modified 2032 coin cells (Herklotz *et al.*, 2016) (experimental details given in Section S2.1) to follow the evolution of the active material ($LiFePO_4$) upon oxidation for a certain galvanostatic current applied between given potential limits. Due to its phase-separating thermodynamics, the oxidation (lithium deintercalation) of $LiFePO_4$ results in the formation of a new phase, heterosite $FePO_4$, with a very similar orthorhombic crystal structure (space group *Pnma*), which starts to nucleate, increasing its phase fraction at the expense of

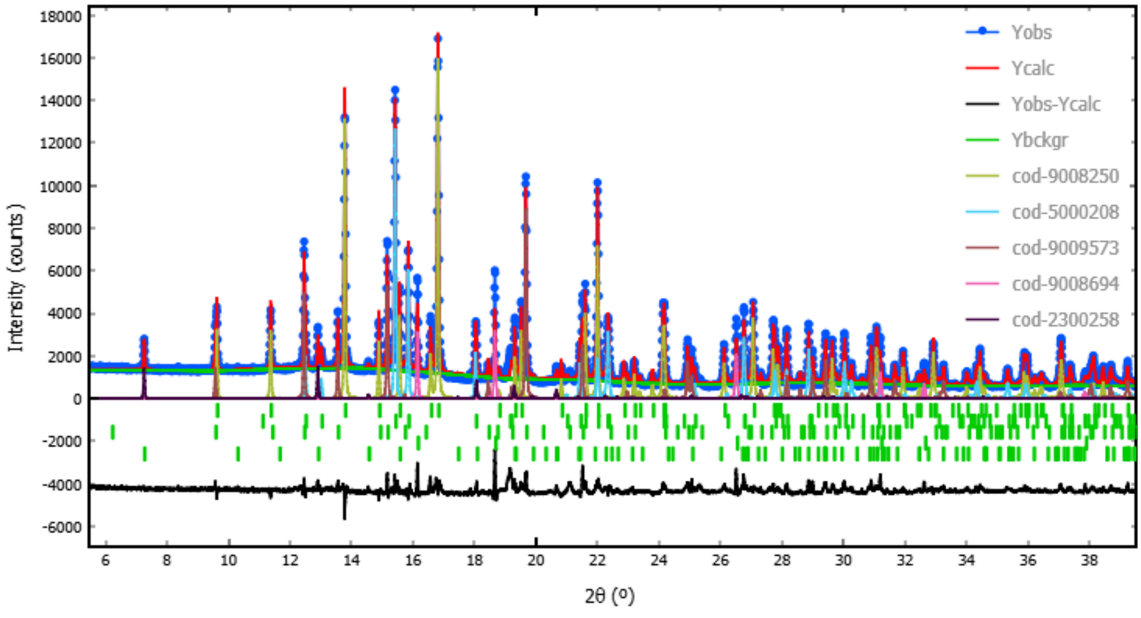


**Figure 2**
Results of the phase search algorithm on the Egyptian makeup samples. $\chi^2 = 7.86$ and $R_{wp} = 14.5$. The experimental X-ray powder diffraction pattern (blue curve) is compared with the calculated profile (red line). The black line denotes the difference curve between them and green vertical lines indicate the Bragg reflections corresponding to each of the identified phases.

$LiFePO_4$. At the end of oxidation only $FePO_4$ is expected to be present. Indeed, the evolving presence of the pair of phases $LiFePO_4$ and $FePO_4$ is visible in the continuous fading of some diffraction peaks and the strengthening of others [Fig. 3(*a*)]. Additionally, a nearly constant signal of the Al current collector is present. Setting up *FullProfAPP* to perform a sequential Rietveld refinement on these data is very straightforward. After downloading and selecting the entries from the COD for the previously mentioned phases $LiFePO_4$ (COD ID 1101111), $FePO_4$ (COD ID 1525576) and Al (COD ID 4313206), the phases are loaded in the 'Automatic Refinement Protocol' window only for the first diffraction patterns in the sequence, while the rest of the patterns are left 'unticked' (Section 2.2.2). The refinement strategy is then selected with the tickable tree items. The refinement parameters are subsequently added to the refinement process in the following six-step workflow: (i) scale factors, (ii) constant $2\theta$ shifts (zero shifts), (iii) background, (iv) cell parameters, (v) strain parameters and (vi) crystallite size parameters. The Al current collector is highly textured and is thus treated with the LeBail

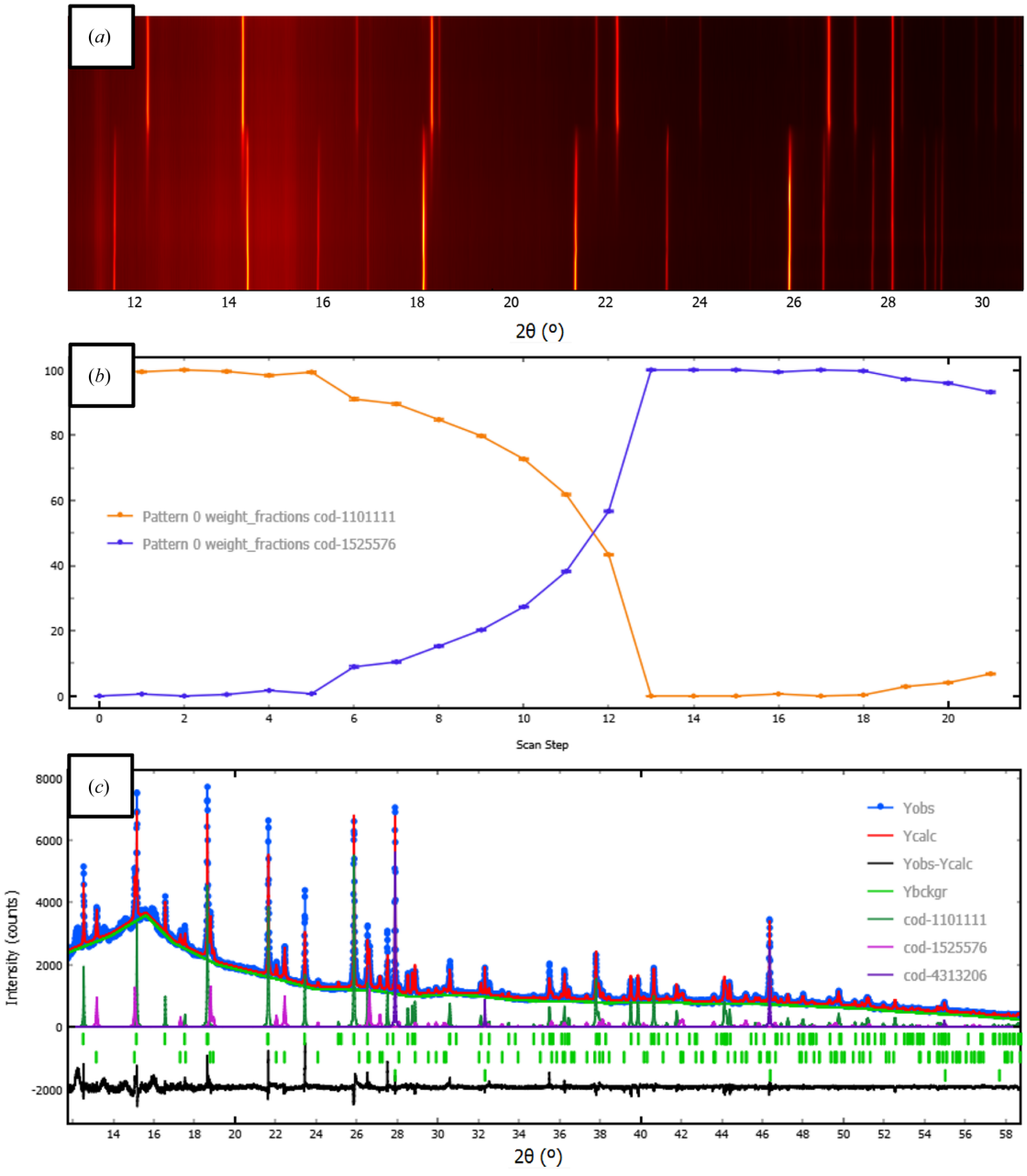


**Figure 3**
(*a*) A contour plot of the $LiFePO_4$–$FePO_4$ synchrotron *operando* data in the 11.5–30.0° $2\theta$ range. (*b*) Evolution of the weight fractions (in wt%) of $LiFePO_4$ (orange) and $FePO_4$ (blue) phases resulting from the automatic sequential Rietveld refinements. (*c*) Results of the calculated profiles with the individual contributions of the phases of the tenth pattern in the sequence. The experimental X-ray powder diffraction pattern (blue curve) is compared with the calculated profile (red line). The black line denotes the difference curve between them and green vertical lines indicate the Bragg reflections corresponding to $LiFePO_4$ and $FePO_4$. Green, violet and purple patterns correspond to the individual calculated profiles of $LiFePO_4$, $FePO_4$ and Al, respectively. Note that the few unindexed peaks in the 12–16° $2\theta$ range are due to other cell components and were not included in the refinement.

method (Fig. S2). Lastly, the 'Sequential Mode' is activated, asking *FullProfAPP* to run the full sequence of diffraction patterns while monitoring the weight fractions of the selected phases in order to control the refinement of the parameters that are likely to produce divergences.

The refinement of the entire sequence using the above-mentioned six-step workflow is completed in under 5 min, with a sequence $\chi^2$ average of 2.8 and with maximum and minimum values of 1.4 and 4.6, respectively. Fig. 3(*b*) shows the evolution of the weight fractions of $LiFePO_4$ and $FePO_4$, along with a series of patterns corresponding to an oxidation process. Note that these plots are a direct output of *FullProfAPP*, which required minimum editing to be included in Fig. 3(*b*). Note also how, even when refining the cell parameters and the strain (and size) parameters for both $LiFePO_4$ and $FePO_4$, the calculation did not diverge in the regions where the weight fractions were close to zero. Fig. 3(*c*) shows an example of a refined profile for the tenth diffraction pattern in the sequence. Visual inspection shows a good fit of the experimental pattern.

**3.2.2. Delithiation and lithiation of layered $LiNi_{1/3}Mn_{1/3}Co_{1/3}O_2$ under battery operation following a solid solution reaction.** In this experiment we used the *operando* LeRiChe'S Cell Version 2 (Choudhary *et al.*, 2023) on the BL16-NOTOS beamline at the ALBA Synchrotron (experimental details in Section S2.2) to track the temporal evolution of the NMC111 material upon oxidation (delithiation) and reduction (lithiation) processes. In contrast to the $LiFePO_4$ example detailed in Section 3.2.1, the NMC class of materials exhibits a succession of steps involving either the formation of solid solutions or phase transitions, depending on composition (relative amounts of Ni, Mn and Co), temperature and applied currents (Zhou *et al.*, 2016; Wang *et al.*, 2022). Within this example, we followed a full charge/discharge cycle of the *operando* cell, during which we observed a smooth evolution of the diffraction peaks of a single NMC111 phase consistent with a solid solution behaviour [Fig. 4(*a*)]. Constant intensity peaks corresponding to the Al current collector and two Be windows are also present.

The setup for the sequential refinement of the series of patterns is similar to the one described in Section 3.2.1. First, we downloaded the relevant phase data from the COD for NMC111 (COD ID 4002443) and Al (COD ID 4313206) and excluded from the refinement the regions where the peaks corresponding to the Be windows appear. The CIFs are loaded in the 'Automatic Refinement Protocol' only for the first pattern in the sequence (see Section 2.2.2). The refinement strategy is then selected by adding steps to the workflow using the tickable parameter tree (Fig. S2). It consists of eight steps: (i) scale factors, (ii) constant $2\theta$ shifts (zero shifts), (iii) background, (iv) cell parameters, (v) crystallite size parameters and (vi)–(viii) three anisotropic strain broadening parameters of the quartic form related to the Laue class $\bar{3}m1$ as implemented in *FullProf*. These last turned out to be extremely important for the refinement due to the anisotropic volume fluctuations of NMC111 during oxidation and reduction. The Al current collector is highly textured and it is refined with the LeBail method. The 'Sequential Mode' is activated, instructing *FullProfAPP* to copy the refined parameters of the previous pattern to the next one.

The refinement of 20 patterns using the eight-step workflow took approximately 2 min to complete, with a sequence $\chi^2$ average of 13.6 and with maximum and minimum values of 9.7 and 20.2, respectively. Figs. 4(*b*) and 4(*c*) show the evolution of the *c* and *a* cell parameters of NMC111, where the characteristic behaviour of this class of materials is well captured. For example, the *c* cell parameter initially increases from 14.31 to 14.52 Å upon lithium extraction due to the increased electrostatic repulsion between the O anions of adjacent transition metal layers (Wang *et al.*, 2022). Upon further oxidation the *c* cell parameter starts to decrease, from 14.52 to 14.39 Å, indicating a diminishing interlayer distance. In contrast, the *a* cell parameter decreases all along the oxidation process, with a small increase at the end. This behaviour is shown to be fully reversible during the reduction process. Fig. 4(*d*) shows the refinement profile of the sixth pattern in the sequence. A visual inspection reveals a good agreement with the experimental pattern, capturing even the anisotropic broadening of the peaks at high angles, which was attributed to anisotropic strains.

**3.2.3. Lithiation of charged spinel $Li_{1-x}Mn_2O_4$ ($0 \leq x \leq 1$) under battery operation following a mixed mechanism.** This section describes an experiment carried out on the powder diffraction beamline BL04-MSPD at the ALBA Synchrotron (Fauth *et al.*, 2013, 2015) (experimental details in Section S2.3), which follows the evolution of $LiMn_2O_4$ (LMO) upon the second cell cycle during reduction. The redox behaviour of LMO involves a combination of phase separation and solid solution mechanisms, as were outlined in Section 3.2.1 for $LiFePO_4$ and in Section 3.2.2 for NMC. Notably, a visual check of the contour plot illustrated in Fig. 5(*a*) reveals that three distinct phases emerge throughout the reduction process. The reduction of the starting delithiated material ($\lambda$-$MnO_2$ with space group $Fd\bar{3}m$) initiates with the formation of a new spinel phase with the same space group $Fd\bar{3}m$. Upon lithiation this phase displays smoothly evolving diffraction peaks, indicating a solid solution reaction. When the reduction of LMO proceeds beyond a certain threshold a third phase appears, which corresponds to the fully reduced spinel $LiMn_2O_4$ phase ($Fd\bar{3}m$). Note that the oxidation and reduction processes of LMO spinels may also involve forming other secondary phases with space groups $P6_3mc$ (Palacín *et al.*, 2000; Dupont *et al.*, 2000) and $P2_13$ (Bianchini *et al.*, 2015). However, it is difficult to extract concrete conclusions about the presence or absence of these phases with the data presented herein. Therefore, the data were fitted by considering spinel LMO phases ($Fd\bar{3}m$) only.

After loading the pattern series and retrieving the phase data from the COD for LMO (COD ID 1514009) and Al (COD ID 4313206), we accommodated the distinct phases that appear along the pattern series using the 'Simulate Selection' button to generate duplicates of the selected CIFs with appropriate starting values for the cell parameters. The setup for the sequential refinement of the diffraction patterns

presented more difficulties than the examples shown in Sections 3.2.1 and 3.2.2 due to the confluence of highly overlapped diffraction peaks with evolving peak positions. In such a scenario, employing a single refinement strategy for the entire pattern series proved unsatisfactory. However, despite the limitations, a stable refinement without divergences was achieved, owing to the systematic addition of refinement parameters and the continuous monitoring of the phase weight fractions. This contrasts with the normal sequential mode available in *FullProf*. Instead, to refine the pattern series effectively, we did the sequential refinement in sections. Initially, focus was directed to the second phase transition

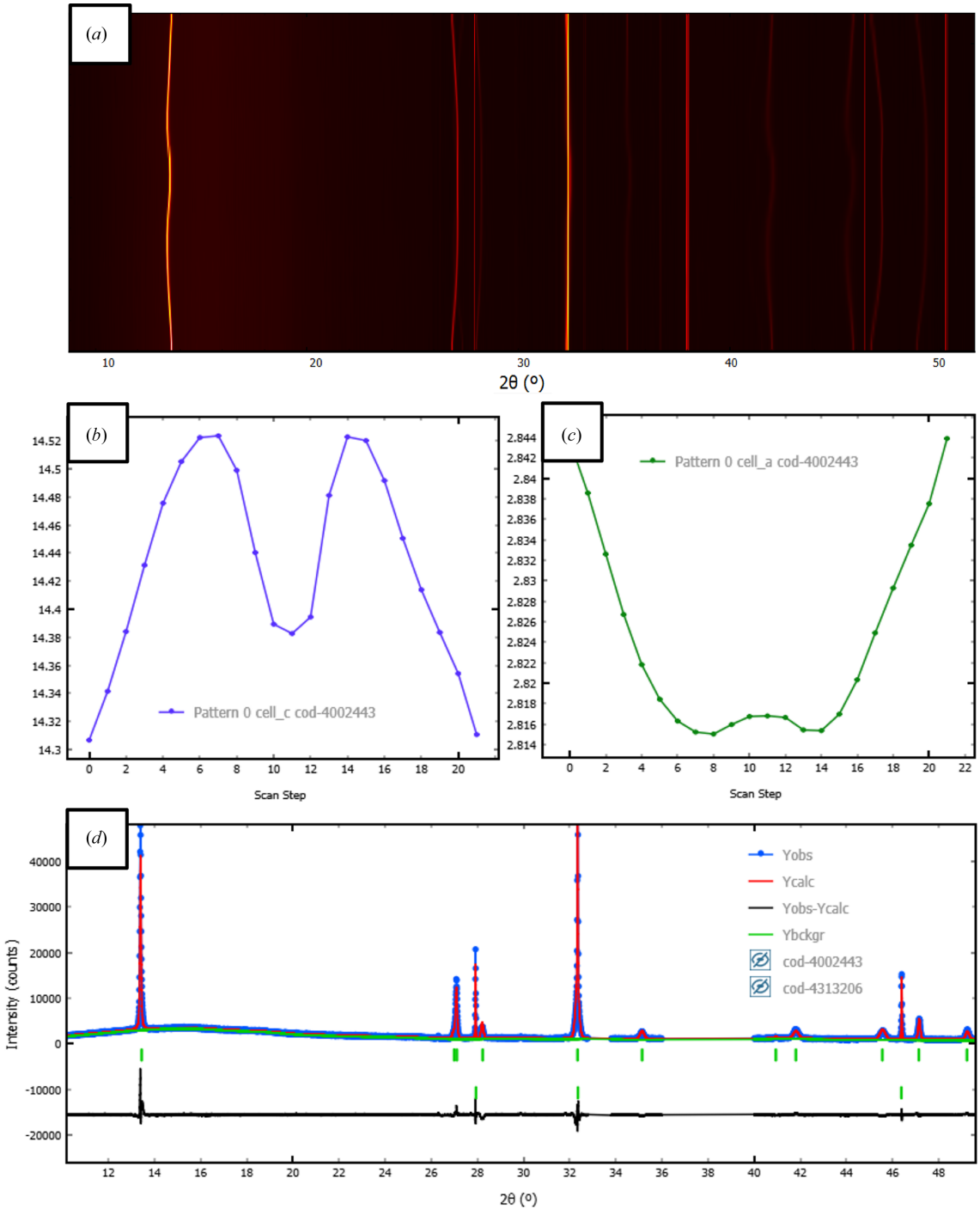


**Figure 4**
(*a*) A contour plot of the NMC111 synchrotron *operando* data in the 8.7–51.6° 2$\theta$ range. (*b*) and (*c*) Evolution of (*b*) the *c* and (*c*) the *a* cell parameters (in ångströms). (*d*) Results of the calculated profiles of the sixth pattern in the sequence. The experimental X-ray powder diffraction pattern (blue curve) is compared with the calculated profile (red line). The black line denotes the difference curve between them and green vertical lines indicate the Bragg reflections corresponding to NMC111 and Al. Note that, as marked in the legend of graph (*d*), the individual contributions of the phases are hidden to improve visibility. *FullProfAPP* allows this to be done by clicking on the legend item itself. All the plots were directly extracted from the GUI and required minimal editing.

region, selecting the pattern where the diffraction peaks appeared clearly distinguished. Using the 'Automatic Refinement Protocol' window, we configured the refinement strategy by subsequently incorporating steps in the workflow using the tickable parameter tree (Fig. S2). The refinement strategy consisted of six steps: (i) scale factors, (ii) constant $2\theta$ shifts (zero shifts), (iii) background, (iv) cell parameters, (v) Lorentzian strain broadening and (vi) Lorentzian size broadening. Fig. 5(*d*) shows the results achieved. To continue analysing the remaining data further, backward and forward sequential refinements were performed starting from this initially refined pattern using the same workflow. In all cases

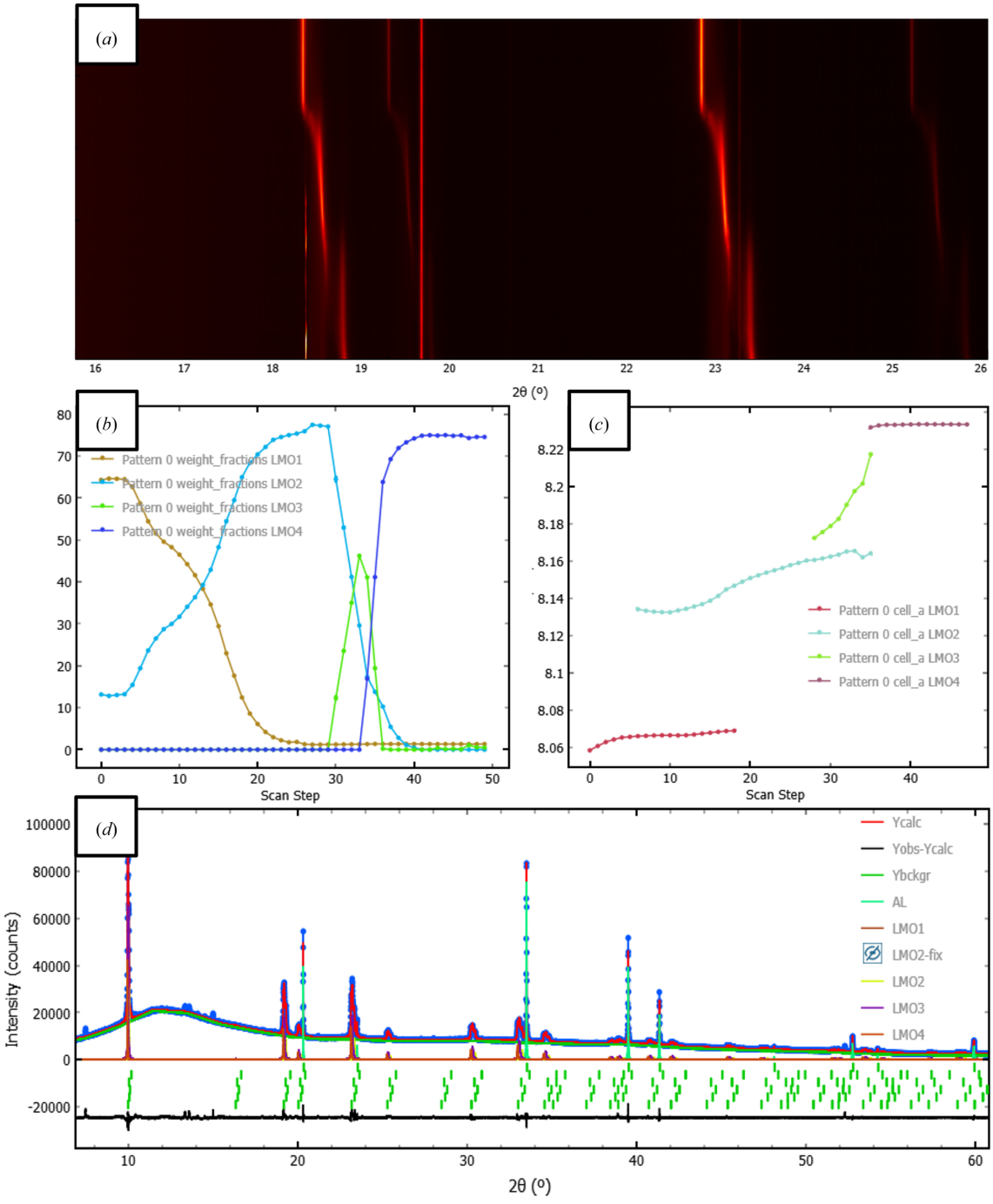


**Figure 5**
(*a*) A contour plot of the LMO synchrotron *operando* data in the 17–26° $2\theta$ range. (*b*) Evolution of the refined weight fractions of the four spinel LMO phases. (*c*) Evolution of the cell parameters (in ångströms) of the four spinel LMO phases. Regions of low weight fraction have been edited out for the sake of visibility and clarity. (*d*) Results of the calculated profiles in the second phase transition region (pattern number 35). The experimental X-ray powder diffraction pattern (blue curve) is compared with the calculated profile (red line). The black line denotes the difference curve between them and green vertical lines indicate the Bragg reflections corresponding to the four spinel LMO phases. Brown, yellow, violet and dun patterns correspond to the calculated profiles of these phases. Note that the few unindexed peaks in the 7–16° $2\theta$ range are due to other cell components and were not included in the refinement.

the Al current collector was refined in LeBail mode. Further sectioning of the pattern series was necessary to refine highly overlapped regions, where the peak broadening parameters were kept constant.

The refinement of the 48 patterns, including the required manual steps, took around 15 min to complete. The sequence $\chi^2$ average was 10.2, with minimum and maximum values of 3.8 and 40.7, respectively. We note that the high $\chi^2$ values were more prominent at the beginning of the reduction process, characterized by intense sharp peaks that could not be assigned to any cell component, and which abruptly appeared and suddenly vanished. In Fig. 5(*b*), the weight fraction

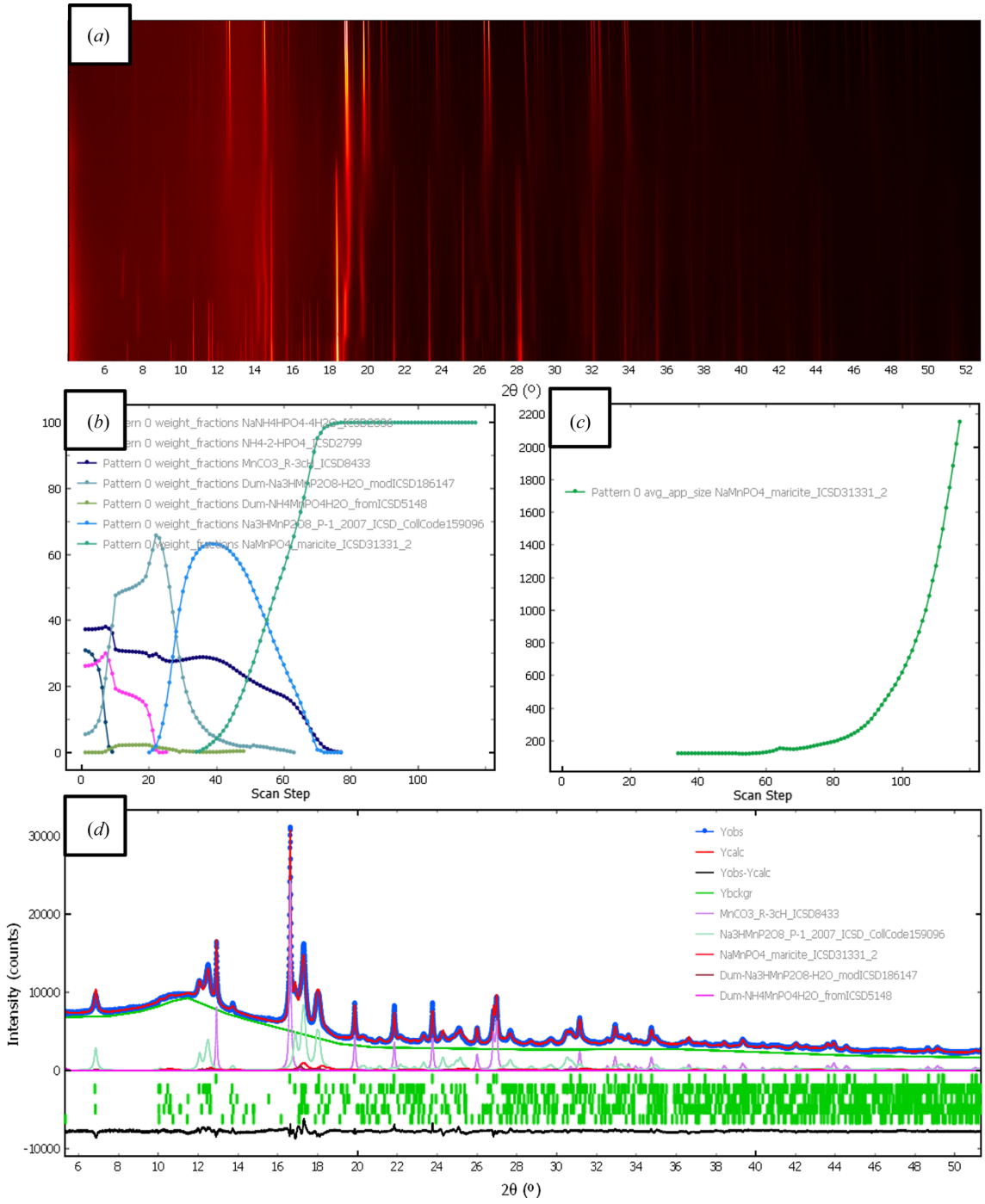


**Figure 6**
(*a*) A contour plot of the evolving diffraction peaks for maricite $NaMnPO_4$ (m-NMP) synthesis with temperature. (*b*) Evolution of the refined weight fractions of the seven indexed phases. (*c*) Evolution of the average apparent size of m-NMP. (*d*) Results of the calculated profiles for a pattern where highly overlapped diffraction peaks exist and where broadening parameters are kept fixed (pattern number 45). The experimental X-ray powder diffraction pattern (blue curve) is compared with the calculated profile (red line). The black line denotes the difference curve between them and green vertical lines indicate the Bragg reflections corresponding to the five identified phases. Light-violet, light-green, red, dark-violet and purple patterns correspond to the calculated profiles of these phases.

evolution for the refined phases across the pattern series is depicted. It illustrates the formation of the three main spinel LMO phases ($Fd\bar{3}m$). However, to describe the second phase transition accurately, an additional spinel phase had to be considered as a short-lived intermediate phase. Its precise origin is unclear and it could simply be due to a delayed solid solution of LMO or inhomogeneities in the active material, but investigating this further is out of the scope of this work. We note that the combined weight fraction of the shown phases does not add up to 100% due to a fixed phase with a 10–15% weight fraction that was considered to represent inactive particles within the cell. Fig. 5(*c*) shows the evolution of the cell parameters for the four cubic phases observed throughout the pattern series. The reduction of LMO results in lithium intercalation, which leads to an increase in cell parameters for LMO phases. Our results agree well with the results reported in other *operando* studies (Sun *et al.*, 2002).

**3.2.4. Maricite $NaMnPO_4$ solid-state synthesis.** In this example (experimental details in Section S2.4), we quantitatively follow the temporal evolution of the reactants, intermediates and final products of the maricite $NaMnPO_4$ (m-NMP) synthesis process during a temperature ramp. Following the previous examples, we first loaded the pattern series, extracted the information about the background and downloaded the corresponding CIFs for all the constituent phases. Guided by visual checks on the low-angle characteristic diffraction peaks [Fig. 6(*a*)], we used *Diffrac.EVA* and the COD and PDF-2 2022 (International Centre for Diffraction Data, Pennsylvania, USA; https://www.icdd.com) databases to index a total of seven candidate phases that appear along the pattern series. The diffraction peaks of the patterns at 30°C were described by the phases $MnCO_3$ ($R\bar{3}c$; ICSD refcode 8433; Inorganic Crystal Structure Database, FIZ-Karlsruhe, Germany; https://icsd.fiz-karlsruhe.de/index.xhtml), $Na(NH_4)H(PO_4)\cdot 4H_2O$ ($P\bar{1}$) (ICSD refcode 2036) and $(NH_4)_2(HPO_4)$ ($P2_1/c$) (ICSD refcode 2799), formed after an initial reaction of $Na_2CO_3$ and $NH_4H_2PO_4$ during the ball-milling step. Similarly, the diffraction peaks at 600°C were also well described with the maricite $NaMnPO_4$ phase (*Pmnb*) (ICSD refcode 31331). To index the three remaining intermediates we used the low-angle characteristic peaks as a reference [Fig. 6(*a*)] and assigned them to $Na_3HMnP_{1.8}O_8$ ($P\bar{1}$) (ICSD refcode 159096), a hypothetical phase $Na_3HMnP_2O_8\cdot\frac{1}{2}H_2O$ isostructural to $Na_3HZrSi_2O_8\cdot(H_2O)_{0.525}$ ($C2/m$) (ICSD refcode 186147) and an intermediate phase $(NH_4)Mn(PO_4)\cdot H_2O$ isotructural to $(NH_4)Mg(PO_4)\cdot H_2O$ ($Pmn2_1$) (ICSD refcode 5148).

The setup of the sequential refinement of the 119 diffraction patterns again required some degree of manual intervention, like the case presented in Section 3.2.3. Again, we divided the pattern series into sections and manually refined specific patterns where the contributions of the individual phases were clearly distinguishable. Backward and forward sequential refinements were then performed starting from these well defined points. Following the previous sections, we set up a six-step refinement workflow: (i) scale factors, (ii) constant $2\theta$ shifts (zero shifts), (iii) background, (iv) cell parameters, (v) Lorentzian strain broadening and (vi) Lorentzian size broadening. To keep the refinement results consistent, the size and strain broadening parameters of low-crystallinity intermediates were kept constant when their contributions became masked by significantly broadened peaks.

The refinement of the entire series took approximately 1 h to complete. The sequence $\chi^2$ average was 8.6, with minimum and maximum values of 3.1 and 18.3, respectively. Fig. 6(*b*) shows the evolution of the weight fractions of the seven phases that we indexed and refined. At 30°C the three reactant phases appear in approximately equal proportions. Immediately after, at ∼70°C, the first intermediate starts forming, corresponding to the hydrated phosphate $Na_3HMnP_2O_8\cdot\frac{1}{2}H_2O$ ($C2/m$). We note that this intermediate phase is already present in small amounts at 30°C. We also note the formation of a minority phase $(NH_4)Mn(PO_4)\cdot H_2O$ ($Pmn2_1$). Then, when the temperature increases to ∼170°C, the $Na_3HMnP_2O_8\cdot\frac{1}{2}H_2O$ ($C2/m$) phase transforms into the $Na_3HMnP_{1.8}O_8$ ($P\bar{1}$) dehydrated intermediate, which becomes the majority phase until it reacts with the remaining $MnCO_3$ ($R\bar{3}c$) at ∼300°C to form the final maricite $NaMnPO_4$ (*Pmnb*). Finally, upon temperature increase to 600°C, m-NMP continues to crystallize, showing a steady increase in the average apparent size with a minimum at 130 Å and a maximum at 2160 Å [Fig. 6(*c*)]. Note that Fig. 6(*c*) features a long tail at low temperature where the value of the average apparent size remains unchanged. This is one of several such examples where the contribution of the m-NMP phase to the diffracted intensity is masked under broad peaks [Fig. 6(*d*)], making the refinement of the broadening parameters difficult. It also signals that the m-NMP crystals do not grow until a threshold temperature of ∼350°C is achieved.

## 4. Conclusions

This article provides an overview of *FullProfAPP*, a GUI that utilizes *FullProf* as the refinement engine. *FullProfAPP* provides a high-level abstraction layer, enabling users to execute different flexible refinement strategies. These strategies facilitate a variety of tasks such as full-profile phase searches and automatic refinements. *FullProfAPP* enables users to perform highly automated data treatment and Rietveld refinements on large batches of data in a simple and intuitive way, while still allowing interaction with the files generated by *FullProf*.

To illustrate the capabilities of *FullProfAPP*, we have introduced several examples, different in nature and covering some, but not all, potential use cases. For example, we show that *FullProfAPP* correctly distinguishes the five constituent phases in an Egyptian makeup sample out of a pool of 366 candidates in a few minutes. It is also able to perform sequential refinements of powder diffraction data from electrochemical *operando* experiments with flexible workflows and parameter monitoring, largely preventing divergences. We tested three common cases where the electrode materials evolve through very different redox mechanisms involving the formation of a secondary phase ($LiFePO_4$), of a solid solution

(NMC111) or a combination of the two (LMO). We additionally examined a complex case, where we tracked the evolution of the different phases observed during the *in situ* monitoring of the solid-state synthesis of m-NMP. In all cases, the setup of the sequential refinements using *FullProfAPP* was very straightforward and the complete pattern series were efficiently refined in minutes. The last two cases proved to be more difficult due to the confluence of overlapped diffraction peaks and evolving peak positions. Nonetheless, satisfactory results were obtained with minimal manual intervention.

All in all, *FullProfAPP* could be useful to those users who routinely deal with large volumes of data, helping them reduce the delay between data collection and analysis time, and thus assisting, for example, on-site scientific and technical decisions on synchrotron experiments. Additionally, it can serve as an entry point for novice users, by reducing the entrance barrier to the full functionality of the *FullProf Suite*.

The program is distributed under an open-source GPLv3 licence with installers for Windows and Linux operating systems.

## 5. Related literature

For further literature related to the supporting information, see Järvinen (1993), Rodriguez-Carvajal *et al.* (1991), Stephens (1999) and Thompson *et al.* (1987).


## Acknowledgements

The authors are indebted to the ALBA synchrotron for granting beamtime on BL04-MSPD (in-house beamtime, and proposal Nos. 2018082922, 2021125510 and 2022025564) and BL16-NOTOS (proposal Nos. 2022035853 and 2022045860), and to the beamline scientists (Giovanni Agostini and Carlos Escudero) for conceiving the experiments and for their assistance during data acquisition. The authors also thank Ainhoa Bustinza, Carlos Berlanga, Montserrat Galceran, Iciar Monterrubio, Joseba Orive, Damien Saurel, María Jauregui, Marcus Fehse and Raphaëlle Houdeville for their assistance in experiments whose data are here refined with *FullProfAPP* to illustrate the capabilities of the program.

## Funding information

This work has received funding from the European Union's Horizon 2020 research and innovation programme under grant agreement No. 957189 (BIG-MAP). The project is part of BATTERY 2030+, the large-scale European research initiative for inventing the sustainable batteries of the future. D. Chatzogiannakis acknowledges the DESTINY MSCA PhD Programme (grant GA 945357). M. Reynaud, J. Carrasco and M. Ismail acknowledge funding from MCIN/AEI/10.13039/501100011033 and 'ESF Investing in your future' for the R&D&I project ION-SELF PID2019-106519RB-I00, and the PhD grant PRE2020-09297. ICMAB-CSIC members thank the Spanish Agencia Estatal de Investigación Severo Ochoa Programme for Centres of Excellence in R&D (grant No. CEX2019-000917-S).


## References


Andersen, C. W., Armiento, R., Blokhin, E., Conduit, G. J., Dwaraknath, S., Evans, M. L., Fekete, Á., Gopakumar, A., Gražulis, S., Merkys, A., Mohamed, F., Oses, C., Pizzi, G., Rignanese, G.-M., Scheidgen, M., Talirz, L., Toher, C., Winston, D., Aversa, R., Choudhary, K., Colinet, P., Curtarolo, S., Di Stefano, D., Draxl, C., Er, S., Esters, M., Fornari, M., Giantomassi, M., Govoni, M., Hautier, G., Hegde, V., Horton, M. K., Huck, P., Huhs, G., Hummelshøj, J., Kariryaa, A., Kozinsky, B., Kumbhar, S., Liu, M., Marzari, N., Morris, A. J., Mostofi, A. A., Persson, K. A., Petretto, G., Purcell, T., Ricci, F., Rose, F., Scheffler, M., Speckhard, D., Uhrin, M., Vaitkus, A., Villars, P., Waroquiers, D., Wolverton, C., Wu, M. & Yang, X. (2021). *Sci. Data*, **8**, 217.

Atkins, D., Capria, E., Edström, K., Famprikis, T., Grimaud, A., Jacquet, Q., Johnson, M., Matic, A., Norby, P., Reichert, H., Rueff, J.-P., Villevieille, C., Wagemaker, M. & Lyonnard, S. (2022). *Adv. Energy Mater.* **12**, 2102694.

Bianchini, M., Fauth, F., Suard, E., Leriche, J.-B., Masquelier, C. & Croguennec, L. (2015). *Acta Cryst.* B**71**, 688–701.

Castelli, I. E., Arismendi-Arrieta, D. J., Bhowmik, A., Cekic-Laskovic, I., Clark, S., Dominko, R., Flores, E., Flowers, J., Ulvskov Frederiksen, K., Friis, J., Grimaud, A., Hansen, K. V., Hardwick, L. J., Hermansson, K., Königer, L., Lauritzen, H., Le Cras, F., Li, H., Lyonnard, S., Lorrmann, H., Marzari, N., Niedzicki, L., Pizzi, G., Rahmanian, F., Stein, H., Uhrin, M., Wenzel, W., Winter, M., Wölke, C. & Vegge, T. (2021). *Batteries Supercaps*, **4**, 1803–1812.

Choudhary, K., Santos Mendoza, I. O., Nadeina, A., Becker, D., Lombard, T., Seznec, V. & Chotard, J. N. (2023). *J. Power Sources*, **553**, 232270.

Coelho, A. A. (2018). *J. Appl. Cryst.* **51**, 210–218.

Cui, X., Feng, Z., Jin, Y., Cao, Y., Deng, D., Chu, H., Cao, S., Dong, C. & Zhang, J. (2015). *J. Appl. Cryst.* **48**, 1581–1586.

Curtarolo, S., Hart, G. L. W., Nardelli, M. B., Mingo, N., Sanvito, S. & Levy, O. (2013). *Nat. Mater.* **12**, 191–201.

Doebelin, N. & Kleeberg, R. (2015). *J. Appl. Cryst.* **48**, 1573–1580.

Dupont, L., Hervieu, M., Rousse, G., Masquelier, C., Palacín, M. R., Chabre, Y. & Tarascon, J. M. (2000). *J. Solid State Chem.* **155**, 394–408.

Eilers, P. H. C. (2003). *Anal. Chem.* **75**, 3631–3636.

Fauth, F., Boer, R., Gil-Ortiz, F., Popescu, C., Vallcorba, O., Peral, I., Fullà, D., Benach, J. & Juanhuix, J. (2015). *Eur. Phys. J. Plus*, **130**, 160.

Fauth, F., Peral, I., Popescu, C. & Knapp, M. (2013). *Powder Diffr.* **28**, S360–S370.

Flores, E., Mozhzhukhina, N., Li, X., Norby, P., Matic, A. & Vegge, T. (2022). *Chem. Methods*, **2**, e202100094.

Flores-Leonar, M. M., Mejía-Mendoza, L. M., Aguilar-Granda, A., Sanchez-Lengeling, B., Tribukait, H., Amador-Bedolla, C. & Aspuru-Guzik, A. (2020). *Curr. Opin. Green Sustain. Chem.* **25**, 100370.

Gelder, R. de, Wehrens, R. & Hageman, J. A. (2001). *J. Comput. Chem.* **22**, 273–289.

Herklotz, M., Weiß, J., Ahrens, E., Yavuz, M., Mereacre, L., Kiziltas-Yavuz, N., Dräger, C., Ehrenberg, H., Eckert, J., Fauth, F., Giebeler, L. & Knapp, M. (2016). *J. Appl. Cryst.* **49**, 340–345.

Järvinen, M. (1993). *J. Appl. Cryst.* **26**, 525–531.

Jennings, S. (2021). *Powder Diffr.* **36**, 212.

Le Bail, A., Duroy, H. & Fourquet, J. L. (1988). *Mater. Res. Bull.* **23**, 447–452.

Liu, D., Shadike, Z., Lin, R., Qian, K., Li, H., Li, K., Wang, S., Yu, Q., Liu, M., Ganapathy, S., Qin, X., Yang, Q.-H., Wagemaker, M., Kang, F., Yang, X.-Q. & Li, B. (2019). *Adv. Mater.* **31**, 1806620.

Lombardo, T., Duquesnoy, M., El-Bouysidy, H., Årén, F., Gallo-Bueno, A., Jørgensen, P. B., Bhowmik, A., Demortière, A., Ayerbe, E., Alcaide, F., Reynaud, M., Carrasco, J., Grimaud, A., Zhang, C., Vegge, T., Johansson, P. & Franco, A. A. (2022). *Chem. Rev.* **122**, 10899–10969.

Lutterotti, L. (2010). *Nucl. Instrum. Methods Phys. Res. B*, **268**, 334–340.

Lutterotti, L., Pillière, H., Fontugne, C., Boullay, P. & Chateigner, D. (2019). *J. Appl. Cryst.* **52**, 587–598.

Palacín, M. R., Chabre, Y., Dupont, L., Hervieu, M., Strobel, P., Rousse, G., Masquelier, C., Anne, M., Amatucci, G. G. & Tarascon, J. M. (2000). *J. Electrochem. Soc.* **147**, 845.

Rietveld, H. M. (1969). *J. Appl. Cryst.* **2**, 65–71.

Rodríguez-Carvajal, J. (1993). *Physica B*, **192**, 55–69.

Rodriguez-Carvajal, J., Fernandez-Diaz, M. T. & Martinez, J. L. (1991). *J. Phys. Condens. Matter*, **3**, 3215–3234.

Rodriguez-Carvajal, J. & Gonzalez-Platas, J. (2002). *Acta Cryst.* A**58**, C87.

Roisnel, T. & Rodríquez-Carvajal, J. (2001). *Mater. Sci. Forum*, **378–381**, 118–123.

Saurel, D., Pendashteh, A., Jáuregui, M., Reynaud, M., Fehse, M., Galceran, M. & Casas-Cabanas, M. (2021). *Chem. Methods*, **1**, 248.

Stephens, P. W. (1999). *J. Appl. Cryst.* **32**, 281–289.

Stier, S., Kreisbeck, C., Ihssen, H., Popp, M. A., Hauch, J., Malek, K., Reynaud, M., Carlsson, J., Gold, L., Goumans, F., Todorov, I., Räder, A., Bandesha, S. T., Wenzel, W., Jacques, P., Arcelus, O., Garcia-Moreno, F., Friederich, P., Maglione, M., Clark, S., Laukkanen, A., Cabanas, M. C., Carrasco, J., Castelli, I. E., Stein, H. S., Vegge, T., Nakamae, S., Fabrizio, M. & Kozdras, M. (2023). *The Significance of Accelerated Discovery of Advanced Materials to Address Societal Challenges*, https://doi.org/10.5281/zenodo.8012140.

Sun, X., Yang, X. Q., Balasubramanian, M., McBreen, J., Xia, Y. & Sakai, T. (2002). *J. Electrochem. Soc.* **149**, A842.

Thompson, P., Cox, D. E. & Hastings, J. B. (1987). *J. Appl. Cryst.* **20**, 79–83.

Tian, P., Zhou, W., Liu, J., Shang, Y., Farrow, C. L., Juhás, P. & Billinge, S. J. L. (2013). *J. Appl. Cryst.* **46**, 255–258.

Toby, B. H. & Von Dreele, R. B. (2013). *J. Appl. Cryst.* **46**, 544–549.

Walter, P., Martinetto, P., Tsoucaris, G., Brniaux, R., Lefebvre, M. A., Richard, G., Talabot, J. & Dooryhee, E. (1999). *Nature*, **397**, 483–484.

Wang, C., Steiner, U. & Sepe, A. (2018). *Small*, **14**, 1802291.

Wang, X., Zhou, H., Chen, Z. & Meng, X. (2022). *Energy Storage Mater.* **49**, 181–208.

Zhou, Y.-N., Yue, J.-L., Hu, E., Li, H., Gu, L., Nam, K.-W., Bak, S.-M., Yu, X., Liu, J., Bai, J., Dooryhee, E., Fu, Z.-W. & Yang, X.-Q. (2016). *Adv. Energy Mater.* **6**, 1600597.